Rydberg states of zinc and measurement of the dipole polarizability of the Zn^+ ion

M. Kompitsas, C. Baharis, and Z. Pan

National Hellenic Research Foundation, Theoretical and Physical Chemistry Institute, 48, Vasileos Constantinou Avenue, 11635 Athens, Greece

Received April 27, 1993; revised manuscript received November 22, 1993

We have recorded the $4sns\ ^1S_0$ ($n = 14$–31), $4snd\ ^1D_2$ ($n = 12$–35), $4snf\ ^{1,3}F^o_J$ ($n = 8$ to $n = 26$), and $4snp\ ^3P^o_{0,1,2}$ ($n = 10$ to $n = 40$) Rydberg series of Zn. We applied various excitation schemes that use two and three laser beams interacting with the Zn vapor in a heat-pipe-like oven with subsequent thermionic detection of the excited states. From the quantum defects of the nonpenetrating $4snf$ levels we estimated the effective dipole polarizability of the Zn^+ core to be $\alpha = 2.30 \pm 0.12 \times 10^{-24}$ cm^3.

1. INTRODUCTION

This paper deals with systematic measurements of Rydberg states of Zn below the first ionization limit. The Zn ground state $4s^2$ consists of two valence electrons outside closed shells. Thus it is homologous to the alkaline-earth atom Ca. In contrast to Ca, the $3d$ subshell of Zn is filled with 10 electrons. This results in significant differences in both the bound and the autoionizing spectra of the two atoms. For example, the Ca doubly excited configurations $3d5s$ and $3d^2\ ^1D_2$ are embedded among the principal series, and they perturb it.[1] This fact enables one to study how the interelectronic correlations manifest themselves in the bound spectrum of Ca. Obviously, this is not the case for Zn. Another perturbing configuration[2] in the bound spectrum of Ca is $4p^2\ ^1S_0$. From early research[3] it is known that the corresponding states for Zn are autoionizing just above the threshold. From our present measurements it is seen that these states can have only a minor effect on the energies of the bound states of the same symmetry.

The first systematic studies on the bound series of Zn involved absorption of Zn atoms in the ground state of light from background continua[4] (microwave-excited rare-gas lamps). The principal $4snp\ ^1P^o_1$ series was observed up to $n = 66$, and from these data the ionization limit was determined to be 75 769.33 cm^{-1}. In the same study[4] the observation of the intercombination lines $4snp\ ^3P^o_1$ to $n = 12$ indicates a slight departure from the pure LS coupling scheme for the Zn atom. Further weak single-photon transitions[4] to $4snd\ ^1D_2$ (for $n \leq 20$) have been attributed to quadrupole transitions.

One should expect that the development of the pulsed dye laser, in combination with multistep excitation schemes, would make detailed studies of Rydberg series possible when the angular momentum J is different from 1, as is the case for the alkaline-earth atoms. The lack of such measurements may be due to the high ionization threshold of Zn and to the fact that the $4s4p\ ^1P^o_1$ resonance transition lies so high that UV tunable radiation near 214 nm is necessary for the first step excitation.

With other than conventional absorption spectroscopy, energy levels and lifetimes of the lowest members of the $4sns\ ^{1,3}S$ and $4snd\ ^{1,3}D$ series have been deduced. Either these levels were populated by an electron impact,[5] or the $4s4p\ ^1P^o_1$ level was populated in a HF discharge and then a laser induced the second step transition.[6] Subsequent decay to the $4s4p\ ^1P^o_1$ level was used for detection. It was claimed[6] that because of the mixing of the autoionizing $4p^2$ configuration with the series studied, the transition matrix element to the $4s4p$ state decreases rapidly, so that for higher n values no detection was possible.

In the present study we overcome the above problems by using a different excitation and detection method, thus extending the measurements to $n = 31$ for the $4sns\ ^1S_0$ and to $n = 35$ for the $4snd\ ^1D_2$ states. The $4s4p\ ^1P^o_1$ state was populated through the decay of the higher-lying $4s5s\ ^1S_0$ state, which was first populated in a two-photon process. To permit detection of the final $4sns$ or $4snd$ state, the atom is ionized either by an ionizing collision or by absorption of a further photon, and the ion is detected in a thermionic detector. The reduced radiative decay rate[6] for higher n favors this detection technique. We have also observed the $4snf\ ^{1,3}F^o_J$ states that were previously unknown, and from their energy positions we have estimated the dipole polarizability α of the Zn^+ core. Finally, we have recorded the $np\ ^3P^o_J$ levels in a three-laser experiment by means of the $4p\ ^3P^o_1$ and $5s\ ^3S_1$ intermediates.

2. EXPERIMENTAL TECHNIQUE

In this experiment, starting from the atomic ground state, the triplet $4snp\ ^3P^o_J$, the singlet $4sns\ ^1S_0$, $4snd\ ^1D_2$, and $4snf\ ^{1,3}F^o_J$ Rydberg series have been recorded and their level energies measured.

Two laser systems were employed. They were driven by a common 10-Hz pulse generator, and the time delay and the sequence of their pulses could be set electronically within a few nanoseconds. The first laser system consisted of a Quantel Nd:YAG laser pumping a Quantel TDL50 dye laser, delivering 8-ns pulses in the visible and near-UV region of the spectrum. The second system con-

0740-3224/94/050697-06$06.00

sisted of a Lumonics excimer laser pumping a Lumonics EPD 300 dye laser. For the three-laser measurements the excimer output was split to pump a home-built dye laser also, which consisted of a Litmann-type oscillator and an amplifier. The system delivered 8-ns pulses with a bandwidth of 0.5 cm^{-1}.

Different types of excitation method involving two- and three-step excitation schemes have been applied, while the laser inducing the last step has been tuned across the spectrum. For wavelength calibration a fraction of the final laser output was sent into a commercial hollow-cathode lamp, and the Ne optogalvanic spectrum[7] was simultaneously recorded. For calibration between the Ne lines another fraction was sent into an evacuated Fabry–Perot interferometer with a 1-cm^{-1} free spectral range, and the transmission fringes were recorded. This method permitted an absolute accuracy of 0.2 cm^{-1} for the final level energy.

The experimental setup is illustrated in Fig. 1. The atomic vapor was confined in a heat-pipe-like oven, which also served as the detector, operating as a thermionic diode. The Zn oven consisted of a cylindrical stainless-steel tube, 42 cm long with a 33-mm internal diameter. The heated zone in the middle was 15 cm long, and the temperature was 420–460 °C, controlled by a NiCr–Ni thermocouple. Two brass cylinders were mounted at both ends of the tube and sealed off by O rings for vacuum purposes. On these cylindrical blocks the entrance windows for the lasers and tap-water tubing for cooling were mounted. On the same blocks the vacuum pipes and the buffer gas line were connected. A few millibars (1 mbar = 7.5 × 10^{-1} Torr) of Ar buffer gas, measured by an MKS Baratron gauge PDR-C-2, was used to reduce vapor diffusion and protect the windows. No systematic shift of the level energies has been detected for this buffer-gas pressure.

The ionization detector consisted of a single stainless-steel wire (34 cm long and 0.3 mm in diameter) stretched off-axis along the tube, operating in the space-charge-limited regime. It was found that at the oven temperature used the wire was not heated enough, and this resulted in a weak signal. So the wire was directly heated by a current of 0.5–1 A. It turned out that the signal was highly sensitive to this current value, that is, to the wire temperature. By a second circuit the wire was negatively biased at 0.8–1.5 V through a 100-kΩ resistor while the tube was grounded. A 20-pF capacitor was used to couple the signal to a linear gate (ORTEC Model 9415), and its output was sent to the chart recorder. The signal was further optimized by positioning of the laser beam ~9 mm from the wire.

3. MEASUREMENTS AND RESULTS

A. Singlet 4*sns* and 4*snd* Spectra

For excitation of the 4*sns* $^1S_0$ and 4*snd* $^1D_2$ states a two-step excitation scheme was applied (see Fig. 2). To populate the 4*s*4*p* $^1P_1^o$ state (at 46 745.4 cm^{-1}) in the first step, a wavelength near 213 nm was needed, which was not available. Therefore we populated this state by first exciting the higher-lying 4*s*5*s* $^1S_0$ (at 55 789.2 cm^{-1}) in a two-photon nonresonant process (λ_1 = 3585 Å), which decayed radiatively to the 4*s*5*p* $^1P_1^o$ state. The TDL50 dye-laser beam was set at 7170 Å, frequency doubled in a KDP crystal, and sent, slightly focused, into the Zn oven. The EPD 300 dye-laser beam, counterpropagating to the first beam, was tuned unfocused in the 356–345-nm region to induce the second single-photon transition. A delay of 4 ns between the two laser pulses was set by optimization of the signal.

In Table 1 the energy values of the observed Rydberg series are listed. For the *ns* $^1S_0$ states, new level energy

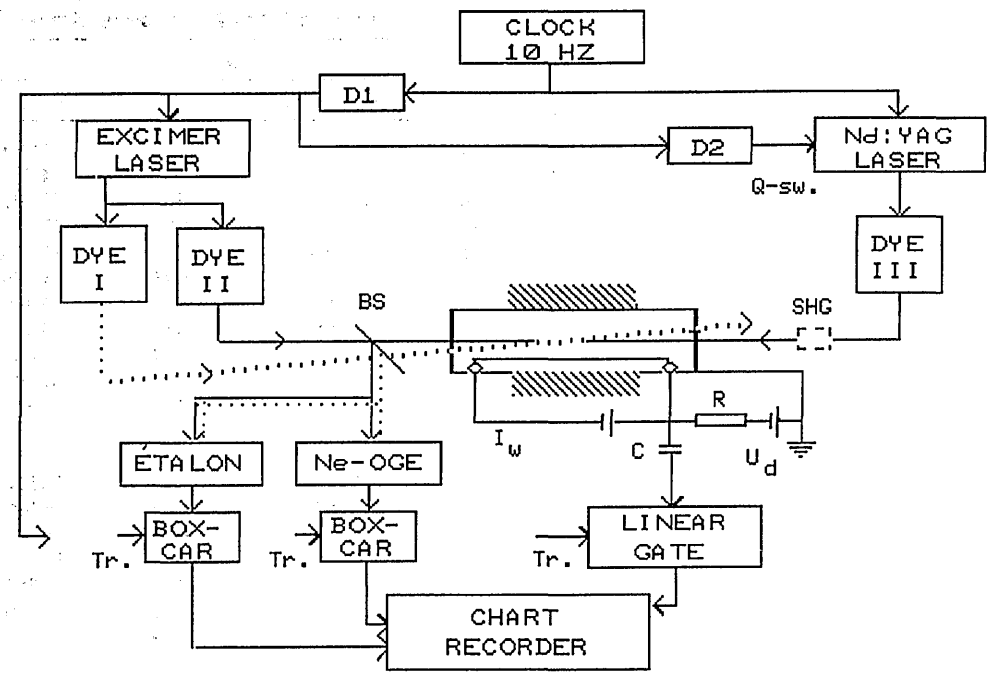

Fig. 1. Block diagram of the experimental arrangement. D1, D2, delays; *Q*-sw., *Q* switching; BS, beam splitter; Tr's, trigger pulses; SHG, second-harmonic-generation crystal; U_d, diode voltage; I_w wire-heating current; R, resistor; C, coupling capacitor; OGE, Ne optogalvanic spectrum.

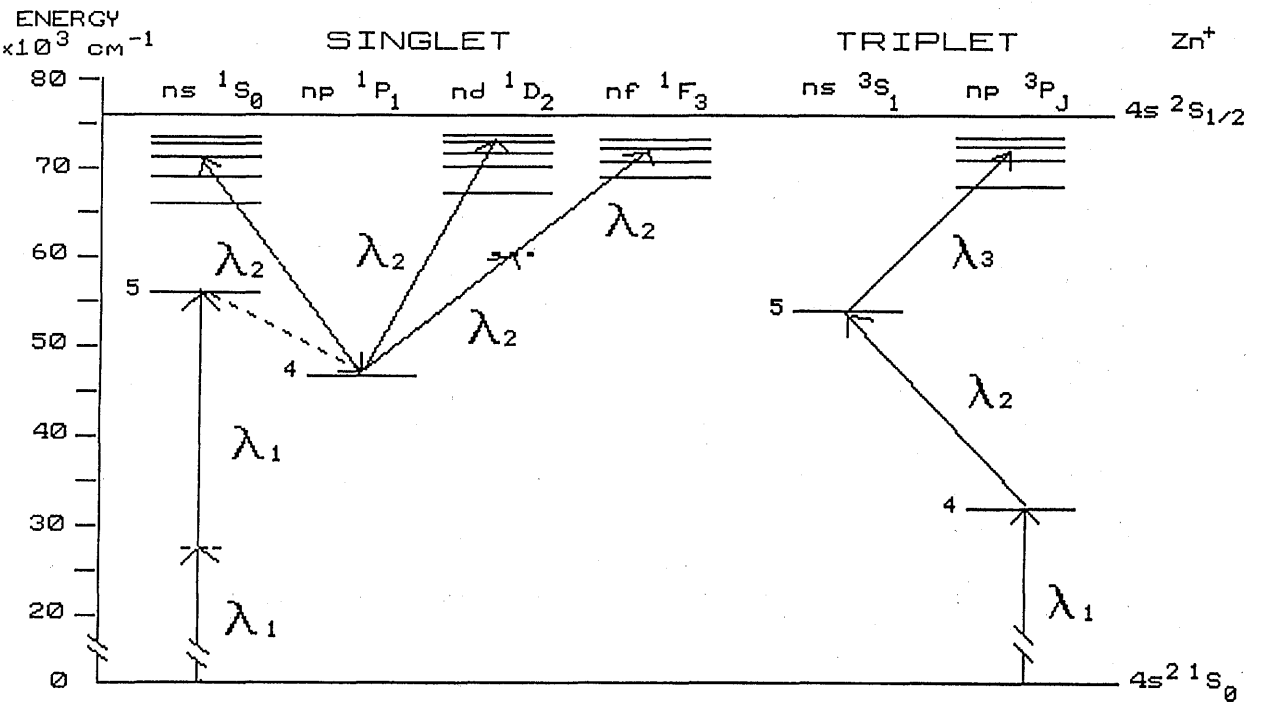

Fig. 2. Part of the Zn spectrum relevant for this experiment, together with the excitation schemes applied. λ_i is the wavelength of the ith step laser.

values are presented here for $n = 14$ to $n = 31$. For $n = 5$ to $n = 9$, energy levels are known from Moore's tables,[8] whereas for $n = 10$ to $n = 12$ they are given by Ref. 6. For the $nd\ ^1D_2$ series energy values for $n = 12$ to $n = 35$ are presented. For $n = 4$ to $n = 20$ our values differ from those of Ref. 4 by 0.2 cm^{-1}, which is within the accuracy of our experiment.

In the third and the fifth column of Table 1 the quantum defects δ of the two Rydberg series calculated according to the modified Rydberg formula,

$$\delta = n - n^* = n - [R/(I - E)]^{1/2}, \qquad (1)$$

are presented. The values for the Rydberg constant R and the threshold I for Zn are those of Ref. 4 and are 109 736.40 cm^{-1} and 75 769.33 cm^{-1}, respectively. The δ values, plotted versus n in Fig. 3 for the ns and in Fig. 4 for the nd series, show no large variations in δ. Thus the series appear to be unperturbed.

B. Singlet–Triplet 4*snf* Spectra

Only the lowest series members, $4f\ ^3F_J^o$ (at 68 833 cm^{-1}), $4f\ ^1F_3^o$ (at 68 835 cm^{-1}), and $5f\ ^1F_3^o$ (at 71 336.15 cm^{-1}), are known[4] thus far. To permit us to record the nf series, the EPD 300 laser induced the first nonresonant transition as above and the TDL50 laser, tunable in the 733–689-nm region, induced the second two-photon $4p\ ^1P_1^o \rightarrow nf$ transition (see Fig. 2). The two linear-polarized laser beams were slightly focused in the center of the oven.

The singlet–triplet splitting of the lowest $4s4f$ configuration[4] is less than 1.5 cm^{-1}. We therefore expect that for the observed $4snf$ levels (for $n = 8$ to $n = 26$), which we present here for what is to our knowledge the first time, the two terms merge into each other and cannot be resolved in this investigation. Indeed, the observed spectrum reveals only one peak for each $4snf$ configuration, and we attribute to it both singlet and triplet characters because, as is stated in Ref. 4, the LS coupling starts to break down for the Zn atom. The series members for $n = 6$ and $n = 7$ have not been recorded: According to our excitation scheme, wavelengths longer than 733 nm were needed, which could not be

Table 1. Observed Lines of the Singlet 4*sns* and 4*snd* Rydberg Series in Zn

	$4sns\ ^1S_0$		$4snd\ ^1D_2$	
n	E (cm^{-1})	δ	E (cm^{-1})	δ
12			74 825.0	1.220
13			74 978.3	1.222
14	74 920.2	2.632	75 097.1	1.223
15	75 051.9	2.632	75 190.8	1.228
16	75 155.1	2.634	75 266.7	1.224
17	75 237.7	2.633	75 328.3	1.226
18	75 304.6	2.633	75 379.3	1.226
19	75 359.7	2.633	75 422.1	1.223
20	75 405.5	2.633	75 458.1	1.223
21	75 444.1	2.631	75 488.7	1.225
22	75 476.7	2.635	75 515.1	1.224
23	75 504.8	2.632	75 537.9	1.225
24	75 528.9	2.636	75 557.7	1.229
25	75 549.9	2.637	75 575.1	1.231
26	75 568.4	2.630	75 590.6	1.221
27	75 584.5	2.634	75 604.1	1.229
28	75 598.8	2.633	75 616.2	1.230
29	75 611.5	2.632	75 627.1	1.223
30	75 622.8	2.634	75 636.8	1.225
31	75 632.9	2.639	75 645.6	1.219
32			75 653.5	1.220
33			75 660.6	1.231
34			75 667.2	1.221
35			75 673.1	1.231

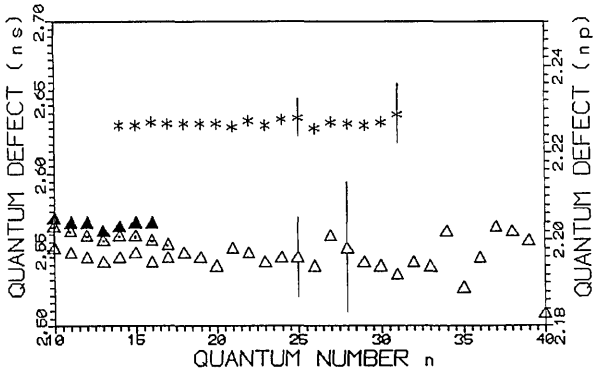

Fig. 3. Quantum-defect plots as a function of the quantum number n. Asterisks, $4sns$ series (left vertical axis); filled triangles, $^3P_0$ levels; triangles with dots, $^3P_1$ levels; open triangles, $^3P_2$ levels of the $4snp$ series (right vertical axis). The error bars are according to Eq. (1) for $\Delta E = 0.2$ cm^{-1} (experimental accuracy).

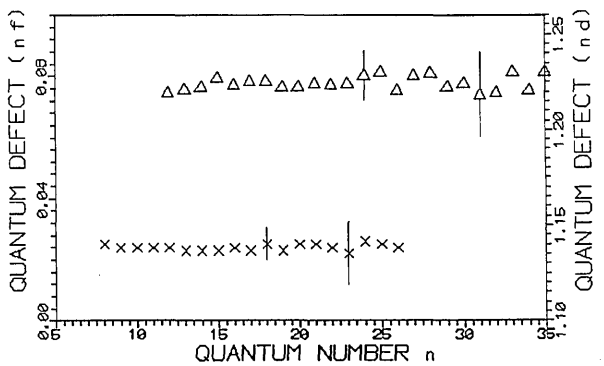

Fig. 4. Same as Fig. 3. Crosses, $4snf$ series (left vertical axis); triangles, $4snd$ series (right vertical axis).

generated by our tunable laser. The level energies E_1 of the $4snf$ $^{1,3}F_J^o$ series are listed in Table 2. The calculated quantum defects for this series ($\delta \simeq 0.024$), in the third column of Table 2, indicate a nonpenetrating orbit and are plotted in Fig. 4. The plot shows that the series is unperturbed.

When we recorded the nd spectra and for $n > 16$, weak peaks appeared systematically at the blue side of each strong nd transition (see Fig. 5). The peak energy values were found to agree, within our accuracy, with the $4s(n-1)f$ level energies, and they are listed, for $n = 19$ to $n = 26$, in the fourth column of Table 2. Owing to their hydrogenic character, higher l states (ng, nh, etc.) are also expected at the same position. Moreover, energy values taken from Ref. 4 show that the $4s(n+1)p$ $^1P_1^o$ states lie energetically between the strong nd transitions and their weak satellites but cannot be resolved in Fig. 5. They may contribute only to the satellites' broadening.

Such weak peaks have also been observed by other authors[9–11] who used devices similar to ours. Systematic studies[9] have shown that the ratio of the satellite to the main peak increases both with the vapor and the buffer-gas density but is independent of other experimental conditions. In a semiquantitative model[9] based on the zero-range Fermi pseudopotential[12] these authors attributed the satellites to the l mixing of the high Rydberg states through collisions of the electron with neutral perturbers. We have not performed such systematic studies in dependence on the Ar pressure but we note that we have observed the satellites at 6 mbar (4.5 Torr), the highest pressure used in the present experiment. A local dc Stark effect caused by space charges in the diode could be another mechanism for inducing l mixing. Which mechanism is mainly responsible for the observed satellites is still an open question, and it can be resolved in a different experiment.

C. Triplet $4snp$ Spectra

For the excitation of the $4snp$ $^3P_J^o$ states, a three-step excitation scheme has been appointed (see Fig. 2). In the first step the $4s4p$ $^3P_1^o$ state was selectively populated by the TDL50 laser beam, which was set to 6154 Å and frequency doubled in a KDP crystal. The homemade dye-laser beam, counterpropagating to the first beam, was tuned to 4723 Å to induce the second step to the $4s5s$ $^3S_1$ state. These two laser beams were linearly polarized horizontally. To populate the final np states, the EPD 300 laser beam crossed the first two beams under a small angle in the center of the oven and was tuned across the 493–452-nm spectral range with the dyes Coumarin 153, 307, and 102. The third laser was linearly polarized vertically. The delays between the laser pulses were set appropriately to maximize the signal. The results are listed in Table 3. All three fine-structure components of the $4snp$ $^3P_J^o$ series have been recorded. Taking into account the polarization directions of the three laser beams, these structures are due to the mixing of the m_J sublevels in the intermediate states through collisions. The triplets have been resolved for $n = 10$ to $n = 17$. For $n = 18$ to $n = 40$ the three levels merge into one; thus no particular value for J is given in the second column of Table 3 and for the δ_{np} value plotted in Fig. 3.

4. DISCUSSION

One may estimate the polarizability α of the ionic core from the quantum defect of the nonpenetrating $4snf$ series. We consider the two-electron system $4snf$ outside closed shells: In the treatment of Van Vleck and

Table 2. Observed Lines of the $4snf$ $^{1,3}F_J^o$ Levels in Zn

	$2h\nu$		$1h\nu$	
n	E_1 (cm^{-1})	δ	E_2 (cm^{-1})	$\lvert E_1 - E_2 \rvert$
8	74 044.1	0.025		
9	74 407.3	0.024		
10	74 666.7	0.024		
11	74 858.5	0.024		
12	75 004.2	0.024		
13	75 117.7	0.023		
14	75 207.6	0.023		
15	75 280.1	0.023		
16	75 339.4	0.024		
17	75 388.6	0.023		
18	75 429.7	0.025		
19	75 464.6	0.023	75 463.7	0.9
20	75 494.3	0.025	75 494.6	0.3
21	75 519.9	0.025	75 519.9	0.0
22	75 542.1	0.024	75 541.9	0.2
23	75 561.5	0.022	75 561.4	0.1
24	75 578.4	0.026	75 578.3	0.1
25	75 593.4	0.025	75 593.5	0.1
26	75 606.7	0.024	75 606.9	0.2

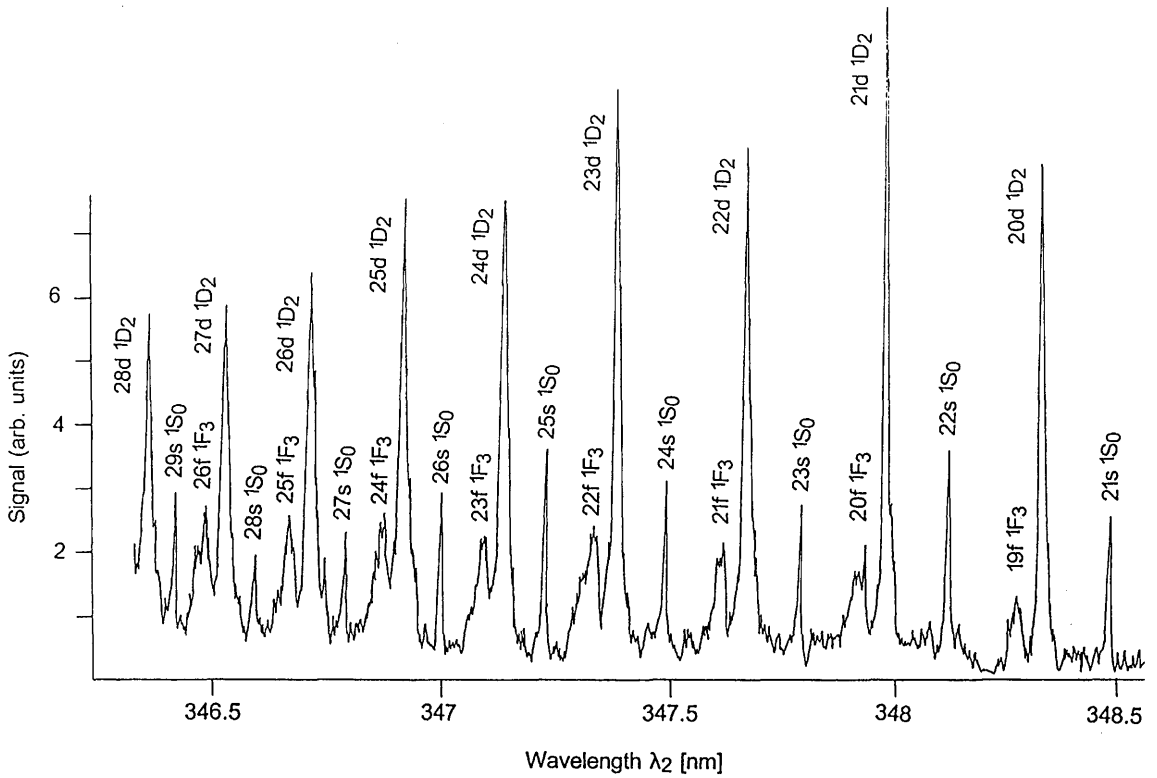

Fig. 5. Part of the $4sns$ and $4snd$ Rydberg spectra. The satellites are resolved as weak peaks on the blue wing of the $(n + 1)d$ transitions. The experimental conditions are $P_{Ar} = 6$ mbar (1 mbar $= 7.5 \times 10^{-1}$ Torr), $U_{diode} = 1.5$ V, $T = 460$ °C.

Whitelaw,[13] the part of the ionic core that is more easily polarized by the outer, nonpenetrating nf electron is the unexcited $4s$ (inner) electron. Briefly, in this model one proceeds as follows: The interelectronic term e^2/r_{ij} is expanded in multipoles, and first the leading (monopole) term is considered in the Hamiltonian only. This means that one approximates r_{ij} by r_o, the radius of the outer electron. The Schrödinger equation is then solved for the two independent electrons. In the next approximation the second (dipole) term in the expansion is considered. This implies that terms leading, e.g., to the quadrupole or higher-order polarizabilities are neglected. In this approximation, perturbation theory leads to the following expression for the term energy W:

$$W = W_0 - (1/2)\alpha e^2 \langle n_0 l_o | r^{-4} | n_0 l_0 \rangle , \qquad (2)$$

with

$$\alpha = -2 \sum_n \frac{|\langle 4s|r|np\rangle|^2}{3W(4s \rightarrow np)}$$

dipole polarizability. W_0 has the hydrogenic form $-RZ^2/n^2$ for nonpenetrating orbits, and $W(4s \rightarrow np)$ is the excitation energy of the inner electron to the levels of the principal np series. The average value $\langle r^{-4} \rangle$ is the hydrogenic one[14] for $l_0 = 3$.

To estimate α from Eq. (2), we refer to the following simplifications made in the calculations and ask if they are fulfilled for the present case of Zn:

(a) The core must be in an S state, which is obvious for Zn.

(b) The $4snf$ singlet–triplet splitting leading to term energy shifts is neglected. In Subsection 3.B we showed that this splitting is negligible and can be ignored.

(c) The total energy $W(4snf \rightarrow n'pnl)$ with $l = d$ or $l = g$, which appears in the calculations in the two-independent-electron approximation, is replaced by the core electron transition energy $W(4s \rightarrow n'p)$. It turns out that this is a significant approximation, leading to the simple Eq. (2) for α.

Since the unperturbed energies of the inner and the outer electrons add to the total energy $W(4snf \rightarrow n'pnl)$, approximation (c) implies that the inner-electron transition energies are much larger than the energies of outer-electron transitions to energetically near-lying nd and ng levels. For the present case of the Zn^+ core the lowest $4s \rightarrow 4p\ ^2P$ inner-electron transitions is[8] 48 480.6 cm^{-1}. Our data show that for $n \cong 20$ the transition energies of the outer electrons to nearby nd states are of the order of some hundred of inverse centimeters, whereas to the still unknown ng states the transition energies are expected to be of the same order of magnitude or less. We therefore conclude that condition (c) is also fulfilled. We apply Eq. (2) for $n = 8$ to $n = 26$, using the experimental level energies $4snf$ in Table 2, and deduce an average value for α,

$$\alpha = (2.30 \pm 0.12)10^{-24}\ cm^3 ,$$

or $\alpha = 15.54\alpha_0{}^3$ in units of the Bohr radius.

Table 3. Observed Lines of the Triplet $4snp$ Rydberg Series in Zn

n	J	E (cm^{-1})	δ
10	0	73 963.1	2.205
	1	73 964.1	2.203
	2	73 966.6	2.198
11	0	74 351.0	2.204
	1	74 351.7	2.202
	2	74 353.3	2.197
12	0	74 625.9	2.204
	1	74 626.5	2.201
	2	74 627.7	2.196
13	0	74 828.1	2.202
	1	74 828.6	2.200
	2	74 829.4	2.195
14	0	74 980.8	2.203
	1	74 981.1	2.201
	2	74 981.8	2.196
15	0	75 099.1	2.204
	1	75 099.4	2.201
	2	75 099.9	2.197
16	0	75 192.8	2.204
	1	75 193.1	2.200
	2	75 193.5	2.195
17	1	75 268.4	2.199
	2	75 268.6	2.196
18		75 329.9	2.197
19		75 380.7	2.196
20		75 423.2	2.194
21		75 458.9	2.198
22		75 489.5	2.197
23		75 515.8	2.195
24		75 538.5	2.196
25		75 558.3	2.196
26		75 575.7	2.194
27		75 590.9	2.201
28		75 604.5	2.198
29		75 616.6	2.195
30		75 627.4	2.194
31		75 637.1	2.192
32		75 645.8	2.195
33		75 653.7	2.194
34		75 660.8	2.202
35		75 667.4	2.189
36		75 673.3	2.196
37		75 678.7	2.203
38		75 683.7	2.202
39		75 688.3	2.200
40		75 692.6	2.183

To our knowledge this is the first time that the Zn^+ dipole polarizability has been obtained experimentally. There are no *ab initio* theoretical calculations either, but nevertheless we may compare our result with values for α estimated from different experimental data sets and test the validity of the model used above. The polarizability as defined in Eq. (2) may be related to the oscillator strength f_{ij} of the $4s$ core electron (level i) to the members j of the np principal series by the formula[15]

$$\alpha = \frac{e^2}{m} \sum_j \frac{f_{ij}}{{\omega_{ij}}^2}, \tag{3}$$

where $\hbar\omega_{ij} = W(4s \rightarrow n'p)$ and e and m, respectively, are the electron charge and mass. Equation (3) indicates that each level $n'p$ contributes by an amount $f_{ij}/{\omega_{ij}}^2$ to the total polarizability. With increasing n', these contributions decrease rapidly, owing both to the increased transition frequencies ω_{ij} and to the generally fast-decreasing values of f_{ij}. It is then expected that data for the first few $n'p$ terms will provide a good estimate of α. The contribution of the $4p\ ^2P_{1/2,3/2}$ levels can be calculated from their lifetime,[16] $\tau = 3$ ns, and their energy positions[8] at 48 480.6 and 49 354.4 cm^{-1}. This contribution to α is 1.84×10^{-24} cm^3; this is already 80% of our experimental value. So we believe that our value for α confirms the results (for lifetimes) of other authors.

5. CONCLUSION

We have measured the energies of the Zn Rydberg series $4sns\ ^1S_0$ for $n = 14$ to $n = 31$, $4snd\ ^1D_2$ for $n = 12$ to $n = 35$, $4snf\ ^{1,3}F^o_J$ for $n = 8$ to $n = 26$, and $4snp\ ^3P^o_{0,1,2}$ for $n = 10$ to $n = 40$. The quantum-defect plots show no noticeable perturbation of these series in the energy range studied. From the $4snf$ data we have estimated the $Zn^+(4s)$ dipole polarizability α, which is in good agreement with lifetime measurements from other authors.

REFERENCES

1. P. Esherick, J. A. Armstrong, R. W. Dreyfus, and J. J. Wynne, Phys. Rev. Lett. **36,** 1296–1299 (1976).
2. J. A. Armstrong, P. Esherick, and J. J. Wynne, Phys. Rev. A **15,** 180–196 (1977).
3. W. C. Martin and V. Kaufman, J. Opt. Soc. Am. **60,** 1096–1099 (1970).
4. C. M. Brown, S. G. Tilford, and M. L. Ginter, J. Opt. Soc. Am. **65,** 1404–1409 (1975).
5. A. L. Osherovich, Y. F. Verolainen, and V. I. Privalov, Opt. Spectrosc. (USSR) **46,** 617–619 (1979).
6. M. Chantepie, J. L. Cojan, J. Landais, B. Laniepce, A. Moudden, and M. Aymar, Opt. Commun. **51,** 391–395 (1984).
7. A. R. Striganov and N. S. Sventitskii, *Tables of Spectral Lines of Neutral and Ionized Atoms* (Plenum, New York, 1968).
8. C. E. Moore, *Atomic Energy Levels,* Natl. Standards Ref. Data Ser. Natl. Bur. Standards **35/V.II,** 124–126 (1971).
9. J.-Y. Zhang and K. T. Lu, J. Phys. B **20,** 5065–5077 (1987).
10. D.-H. Wu, Y.-F. Yang, and K. T. Lu, J. Phys. B **23,** L149–L152 (1990).
11. Y. Makdisi and K. S. Bhatia, Can. J. Phys. **68,** 1464–1468 (1990).
12. A. Omont, J. Phys. (Paris) **38,** 1343–1359 (1977).
13. J. H. Van Vleck and N. G. Whitelaw, Phys. Rev. A **44,** 551–569 (1933).
14. H. A. Bethe and E. E. Salpeter, *Quantum Mechanics of One- and Two-Electron Atoms* (Springer-Verlag, Berlin, 1957), Chap. 1, p. 17.
15. I. I. Sobelman, *Atomic Spectra and Radiative Transitions* (Springer-Verlag, Berlin, 1979), Chap. 9, p. 209.
16. T. Andersen, O. Poulsen, and P. S. Ramanujam, J. Quantum Spectros. Radiat. Transfer **16,** 521–527 (1976).